

Relationship between Intensity and Recorded Ground-Motion and Spectral Parameters for the Himalayan Region

by Anbazhagan Panjamani, Ketan Bajaj, Sayed S. R. Moustafa, and Nassir S. N. Al-Arifi

Abstract Empirical relationships between the macroseismic intensity and the ground-motion parameters for the Himalayan region are derived in this study. A strong-motion database from 21 moderate-to-large earthquakes, along with their corresponding macroseismic intensity, is considered. All the intensity values are inferred from isoseismal maps and earthquake damage reports and then converted to the modified Mercalli intensity (MMI) scale. An orthogonal regression analysis is used to find the best correlation between MMI and peak ground acceleration (PGA), peak ground velocity (PGV), and pseudospectral acceleration (PSA) at 0.3, 1.0, 2.0, and 3.0 s to accommodate the uncertainty in the regression coefficients. In addition to the ground-motion parameters, the MMI is related to other potential independent variables, including the moment magnitude, the hypocentral distance, and the 30-m average shear-wave velocity (V_{S30}). The study shows that site effect is noticed predominantly in the MMI–PGA relationship for a hypocentral distance of more than 200 km. When relating MMI with PGV, $PSA_{0.3\text{ s}}$, $PSA_{1.0\text{ s}}$, $PSA_{2.0\text{ s}}$, and $PSA_{3.0\text{ s}}$, however, the contribution of site effects to the correlation is negligible. To eradicate the site effect in the PGA–MMI relationship, the derived empirical relationship is modified, based on the statistical analysis of MMI observed and MMI predicted, with or without including V_{S30} as a potential independent variable. Furthermore, the developed regression models are verified using several statistical tests, the F -test, the t -test, the Durbin–Watson test, and the Breusch–Pagan test. Additionally, the Euclidean distance concept is evaluated in the study. It was concluded that the PGA is a good indicator for deriving the MMI value in the Himalayan region, but that one should use site-specific MMI versus PGV and MMI versus PSA relationships to predict reliable parameters.

Introduction

Macroseismic intensity plays an important role in various seismological, engineering, seismic-hazard, and risk-related studies. It has been used for centuries to characterize the perceived effects of earthquakes for regions for which little or no measured strong-motion database is available. It is also useful in providing information about preinstrument earthquakes, in which the intensity distribution pattern would be useful in loss estimation for future destructive earthquakes (Shah *et al.*, 1991). The macroseismic intensity scale can also be used in interpreting the response of structures, in hazard estimation, and in disaster management planning (Bilal and Askan, 2014). The degree of shaking due to an earthquake event can be estimated either quantitatively in terms of the peak ground parameters or qualitatively using the felt intensity. The felt-intensity values are determined based on the observed structural damage and/or the response of humans to the ground shaking. These felt intensities are useful as an input in rapid loss modeling around the globe in the Prompt Assessment of Global Earthquake for Response

(PAGER) (Earle *et al.*, 2009), the Earthquake Loss Assessment for Response and Mitigation (QLARM) (Trendafiloski *et al.*, 2011), and the Earthquake Loss Estimation Routine (ELER) (Kamer *et al.*, 2009). To date, however, there is no explicit relationship between the macroseismic intensity and the ground-motion parameters for the Himalayan region that can be used in rapid loss estimation in probable future earthquakes. Bilham (2015) highlighted that the 25 April 2015 Gorkha earthquake failed to fully rupture the main fault beneath the Himalayan region, and therefore, a large earthquake appears to be inevitable in the future. Correlation between the peak ground parameters and the intensity would be advantageous in assessing the seismic hazard and the risk of damage, as well as in evaluating historical earthquakes for which recorded ground-motion data are not available (like in India and other Asian countries). This would also be useful in the rapid assessment of the severity due to ground shaking and in developing digital isoseismal maps (Wald *et al.*, 1999).

Previously, researchers have related the modified Mercalli intensity (MMI) to the peak ground acceleration (PGA), because this is significant in seismic-resistant design, as the product of PGA and mass would be useful in assessing the inertial force loading for structures (Gutenberg and Richter, 1956; Hershberger, 1956; Murphy and O'Brien, 1977; McCann *et al.*, 1980). As shown by Kaka and Atkinson (2004), however, the peak ground velocity (PGV) is actually the optimum ground-motion parameter for ShakeMap applications, because the PGV is also directly related to the kinetic energy, which further influences the damage to a structure. Spence *et al.* (1992) concluded that the MMI relates better with spectral accelerations obtained using a 5% damping (mean amplitudes in the 0.1–0.3 s short-period range) than with the PGA. Wald *et al.* (1999) demonstrate that, although low levels of shaking intensity (i.e., between V and VIII) correlate better with both the PGA and the PGV, high intensities (i.e., between V and IX) correlate best with the PGV. Based on the 1994 Northridge earthquake, Boatwright *et al.* (2001) showed that the PGV is significantly better correlated with intensity as compared to the PGA, and also that intensity correlates fairly well at a 5% damped pseudovelocity response spectra at 0.2 s and correlates the best at 1.5 s. Akansel *et al.* (2013), meanwhile, studying the damage due to large earthquakes, concluded that damage to different types of structures can be correlated well with either the PGA or the PGV, depending upon the stiffness of the structure. Bilal and Askan (2014) concluded that MMI relates better with PGV for ductile structures, and brittle structures are PGA sensitive.

Most of the structures near the Himalayan belt or in and around the Indo-Gangetic basin are of mixed type; that is, they are constructed using a mix of traditional and modern construction techniques. Most of these structures are not seismic resistant and may not be ductile. The earthquake loss estimation for the Himalayan region requires a region-specific relationship between intensity and ground-motion parameters. In this study, an orthogonal regression algorithm is used for deriving an empirical relationship between the MMI and the ground-motion parameters such as the PGA, the PGV, and the pseudospectral acceleration (PSA) at 0.3, 1.0, 2.0, and 3.0 s for the Himalayan region. Furthermore, the moment magnitude, the hypocentral distance, and the shear-wave velocity at 30 m depth (V_{S30}) have been incorporated as the potential independent variables in the relationship. This serves the major purpose of eliminating the regional dependency (Bilal and Askan, 2014), and V_{S30} counterbalances the site effect. A new relationship between the PGA and MMI is proposed here to counterbalance the site effects for those regions for which V_{S30} is not available. A statistical analysis is also undertaken for the developed equation to consider the sum of the squares of residuals (SSRs) and a quintile–quintile ($Q-Q$) plot. An analysis of variance (ANOVA) using the F -test, Durbin–Watson test (DW-test) (Durbin and Watson, 1950), and Breusch–Pagan test (BP-test) (Breusch and Pagan, 1979) is carried out to verify and validate

the newly developed model. Additionally, based on the concept of Euclidean distance (ED), the θ value, which is the ratio between the observed and derived ED, is used to compare the observed MMI with the calculated MMI using derived MMI versus ground-motion relationships.

Seismicity of the Study Area and Data

The Indian plate is moving toward the Asian plate at a high rate of 15–20 cm/year (Bilham *et al.*, 1998), which results in collision between these two plates. As a result of this, the state of stress is high in the Indian plate due to crustal shortening along its northern edge, which in turn increases the earthquake hazard, particularly in northern India. This process gives rise to three major thrust planes, the Main Central thrust (MCT), the Main Boundary thrust (MBT), and the Himalayan frontal fault (HFF) (Gansser, 1964; Molnar and Chen, 1982). The Himalayan geodynamics are the cause of great earthquakes: the 1897 Assam (M_w 8.1), the 1905 Kangra (M_w 7.8), the 1934 Bihar–Nepal (M_w 8.0), the 1950 Assam (M_w 8.7), the 2005 Kashmir (M_w 7.6), the 2011 Sikkim (M_w 6.9), and the 2015 Nepal (M_w 7.8) earthquakes. These have been well studied by various researchers (Seeber and Armbruster, 1981; Khattri, 1999; Bilham and Gaur, 2000). A 750-km-long central segment lying between the eastern edge of the 1905 Kangra earthquake rupture zone and the western edge of the 1934 Bihar–Nepal earthquake remains unbroken and is under high strain (Singh *et al.*, 2002). Furthermore, Khattri (1999) has estimated the probability of occurrence of a greater than magnitude 8.5 earthquake in the gap during the next 100 years as 0.59. A recent study by Bilham (2015) on the Gorkha earthquake of 25 April 2015 postulates that northern Nepal shifted up to 7 m southward and Kathmandu rose by 1 m. This study further concluded that this earthquake failed to fully rupture the main fault beneath the Himalaya, and, therefore, a large earthquake is inevitable in the future. A proper study is therefore needed for pre-earthquake damage assessment.

The Department of Earthquake Engineering, Indian Institute of Technology, Roorkee (IITR), has operated a network of about 200 strong-motion accelerographs in the northern and northeastern part of the country since 1976 to understand the seismicity and the seismotectonic characteristics of the strong motion in the Himalayan region. The data used in this study consisted of 21 strong-to-moderate earthquakes occurring in the Himalayan region from 1988 to 2015 with a moment magnitude (M_w) varying from 5.1 to 7.8 and a hypocentral distance (R) between 14.3 and 918.07 km. Data from all of the earthquakes (marked with a circle) and stations (marked as a square) used in this study are shown in Figure 1. Sixty-eight strong ground motions recorded before 2005 were collected from 55 stations that are installed in the Himalayan region to form the Virtual Data Center (VDC). The data obtained from the VDC were baseline corrected and band-pass filtered between 0.75–0.9 and 25–27 Hz. From the 191 ground-motion recordings, 124 were collected from the

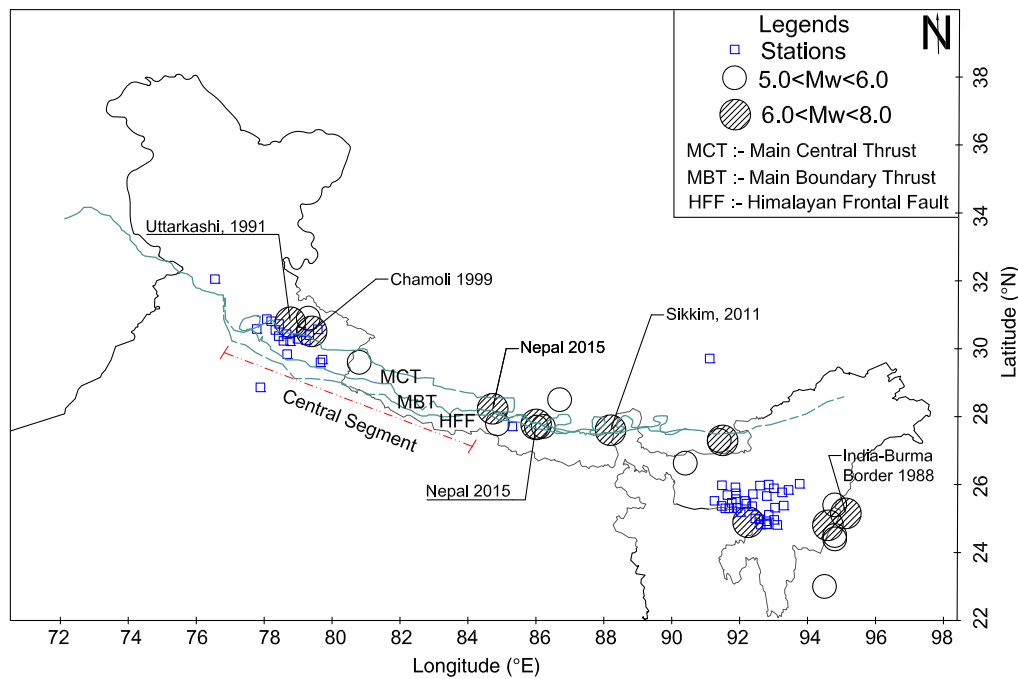


Figure 1. Database for recorded events (marked as circles of different sizes based on magnitude) and the strong-motion instrumentation network (marked as squares) used in the present study. Six major earthquakes having moment magnitudes of more than 6.5, including the recent Nepal 2015 earthquake, are also marked, along with the Main Boundary thrust (MBT), the Main Central thrust (MCT), and the Himalayan frontal fault (HFF) (after Kayal, 2008) and the central segment (after Rajendran *et al.*, 2015). The color version of this figure is available only in the electronic edition.

strong-motion instrumentation network of the IITR covering the Indian Himalayan range from Jammu and Kashmir to Meghalaya (the details of these data are given in [Data and Resources](#)). The database obtained from the IITR was baseline corrected, and because the natural frequencies of the sensors are high, instrumentation correction was not required. Details about the strong-motion instrumentation network are given in [Kumar *et al.* \(2012\)](#). The waveform obtained was high-pass filtered at a 0.5–0.8 Hz corner frequency and low-pass filtered at 25 Hz using a fourth-order Butterworth filter. The processed acceleration time history was further integrated to obtain the velocity time history and spectral acceleration at various time periods.

In the present study, intensity was obtained from isoseismal maps and past earthquake damage reports. The majority of the isoseismal maps used in this study were taken from [Kayal \(2008\)](#). These maps were developed by means of a detailed postearthquake survey conducted by a reconnaissance team. Most of the isoseismal maps of recent earthquakes are expressed in terms of the MMI only, although for a few earthquakes, isoseismal maps have been developed using the Medvedev–Sponheuer–Karnik (MSK) scale and the European Macroseismic Scale (EMS). To derive the relationship between macroseismic intensity and ground-motion parameters, different macroseismic intensities are converted into a single intensity scale, that is, the MMI following [Musson *et al.* \(2010\)](#). As per [Musson *et al.* \(2010\)](#) and [Reiter \(1990\)](#), the MMI and the MSK are the same on both an empirical and a theoretical basis. The conversion table given

by [Musson *et al.* \(2010\)](#) was used here to convert the different intensity scales to MMI. For the 1999 Chamoli earthquake, the isoseismal map used in this study is taken from [Mahajan and Viridi \(2001\)](#), with the published isoseismal map being both in MSK scales and EMS. In a few studies of historical earthquakes ([Kaka and Atkinson, 2004](#)), the MMI versus PGA relationships were developed by taking the PGA, the PGV, and the PSA values from the ground-motion prediction equation developed for that particular region. In the present study, however, only those data with the observed macroseismic intensity and the PGA, the PGV, and the PSA values at the same location were used. Additionally, for the recent 2015 earthquakes and a few Indo-Burmese earthquakes for which isoseismal maps or damage reports are not available, the MMI data were compiled from the “Did You Feel It?” (DYFI) website (see [Data and Resources](#)). DYFI ([Wald *et al.*, 1999](#)) is an internet-based questionnaire from the U.S. Geological Survey (USGS) website. DYFI plays an integral role in many postearthquake assessments and is an important communication tool in engineering seismology. As in [Atkinson and Wald \(2007\)](#) and [Wald *et al.* \(2011\)](#), the DYFI database is a useful and reliable tool for the detection of intensity variability in a region. The DYFI data have been used by various researchers ([Atkinson and Kaka, 2007](#); [Worden *et al.*, 2012](#); [Bilal and Askan, 2014](#); [Caprio *et al.*, 2015](#)) for deriving the relationship between the MMI and the ground-motion parameters.

Because macroseismic intensity is based either on the observed structural damage or the response of humans to ground shaking, the local site effects need to be included

Table 1

The Number of Data Points Used in This Study Regarding MMI and Recorded PGA, PGV, PSA, and V_{S30} Corresponds to Different Hypocentral Distance and Magnitude

Serial Number	Earthquake Name	Event Date (yyyy/mm/dd)	Latitude and Longitude (° N)–(° E)	Magnitude	Number of MMI–PGA, PGV, and PSA Pairs	Number of V_{S30} Pairs	Distance Range (km)
1	India–Burma border	1988/08/16	25.15–95.13	7.3	33	24	189.9–400.2
2	Uttarkashi	1991/10/19	30.78–78.77	7	13	10	21.7–153.5
3	India–Myanmar border	1997/05/08	24.89–92.25	6	11	11	41.9–125
4	Chamoli	1999/03/28	30.51–79.4	6.6	11	6	17.3–160
5	Chamoli	2005/12/14	30.9–79.3	5.2	8	7	54.29–190.18
6	Bhutan	2009/10/29	27.3–91.4	5.2	5	5	124.01–231.04
7	Myanmar	2009/08/11	24.4–94.8	5.6	12	12	207.65–507.22
8	Myanmar–India border	2009/12/29	24.5–94.8	5.5	6	6	227.08–478.97
9	Manipur–Meghalaya border	2009/08/30	25.4–94.8	5.3	5	4	145.31–459.97
10	Bhutan	2009/09/21	27.3–91.5	6.2	14	12	125.82–321.5
11	Myanmar	2010/03/12	23.0–94.5	5.6	5	5	271.63–554.34
12	Tibet	2010/02/26	28.5–86.7	5.4	7	6	222.73–560.61
13	India–Myanmar	2011/02/04	24.8–94.6	6.4	7	6	221.37–544.42
14	Sikkim	2011/09/18	27.6–88.2	6.8	13	11	50.34–918.07
15	Nepal border	2011/04/04	29.6–80.8	5.7	24	19	39.36–484.54
16	Basugaon	2015/06/28	26.63–90.4	5.1	3	3	189.3–516.8
17	Nepal border	2015/04/25	27.79–84.87	5.1	3	3	46.2–644.8
18	Kodari, Nepal	2015/05/12	27.71–86.22	5.5	3	3	47.2–559.6
19	Kodari, Nepal	2015/04/25	27.69–86.02	5.6	3	3	68.6–624.4
20	Nepal border	2015/05/26	27.77–86.01	6.7	3	3	64.9–622.3
21	Nepal	2015/04/25	28.23–84.73	7.8	2	2	14.3–518.4

MMI, modified Mercalli intensity; PGA, peak ground acceleration; PGV, peak ground velocity; and PSA, pseudospectral acceleration.

when deriving the intensity from any ground-motion parameter. In the present study, average shear-wave velocity values up to a depth of 30 m (V_{S30}) were calculated for different sites based on the relationship proposed by Ghofrani and Atkinson (2014). Ghofrani and Atkinson (2014) evaluated a peak frequency and peak amplitude from the horizontal-to-vertical spectral acceleration ratio (HVSAR) from several earthquakes and related it to known V_{S30} values for different sites. The V_{S30} values derived using the relationship proposed by Ghofrani and Atkinson (2014) were within a factor of 1.41 (0.15 log units), but only for the sites with a peak frequency greater than or equal to 1 Hz.

To homogenize the database, certain criteria were applied. First, the ground-motion parameter was selected as the larger of the two horizontal components. Second, the distance between the reported MMI and the ground-motion parameters was set at less than 1 km. Finally, the MMI and V_{S30} assigned to the various stations were within a standard deviation of ± 1 and ± 1.41 , respectively. The 21 earthquakes used in this study had uniform macroseismic intensities in the MMI scale and the ground-motion parameters of the PGA, the PGV, and the PSA at 0.3, 1.0, 2.0, and 3.0 s. Therefore, the 191 intensity measurements were paired with 191 ground-motion parameters. From this dataset of 191 readings, however, only 161 locations have a peak frequency greater than or equal to 1 Hz; therefore, the V_{S30} values are calculated for those sites only (as explained above). A summary of felt intensity for the events and the recorded ground-motion parameters used in the study is given in Table 1. Further, the scatter-plot matrix of the database used in this study is given in Fig-

ure 2, showing the distribution and correlation of the MMI, the magnitude (MAG), the hypocentral distance (HYPO), the PGA, the PGV, and the PSA at 0.3, 1.0, 2.0, and 3.0 s. The diagonal of each matrix shows the distribution of the parameter and the crossing line, and the columns display the scatter in the upper triangular matrix and the correlation values in the lower triangular matrix. For example, row 1 and column 2 show the scatter plot between the MMI and the MAG, whereas row 2 and column 1 show the correlation value of 0.57. Similarly, row 1 and column 7 show the scatter plot between the MMI and the $PSA_{1.0s}$, whereas row 7 and column 1 show the correlation value of 0.62.

Regression Analysis and Model Verification Test

The three regression models used in the study are

$$MMI = a + b \log(X) + \sigma \tag{1}$$

$$MMI = a + b \log(X) + cM_w + d \log(R) + \sigma \tag{2}$$

$$MMI = a + b \log X + cM_w + d \log R + e \log(V_{S30}) + \sigma, \tag{3}$$

in which X corresponds to PGA, PGV, $PSA_{0.3s}$, $PSA_{1.0s}$, $PSA_{2.0s}$, $PSA_{3.0s}$ (the PSA subscript indicates the period), and σ is the standard error in the MMI. In the above equations, a is an intercept, and b , c , d , and e are the regression

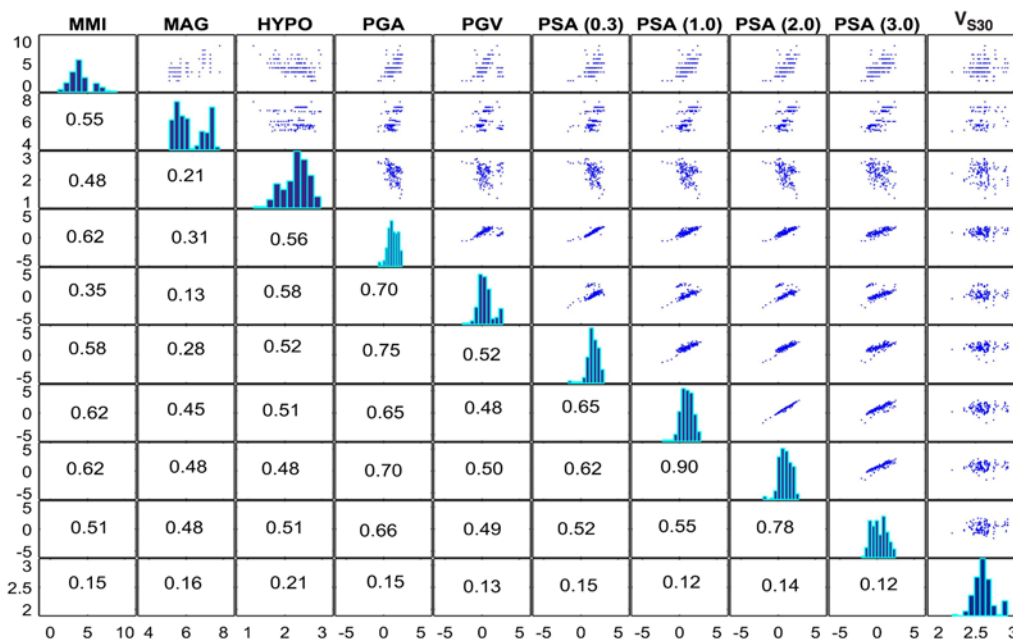


Figure 2. Scatter plot of the data used in this study with distribution and correlation of the modified Mercalli intensity (MMI), the magnitude (MAG), the hypocentral distance (HYPO), peak ground acceleration (PGA), peak ground velocity (PGV), and pseudospectral acceleration (PSA) at 0.3, 1.0, 2.0, and 3.0 s. The upper triangular matrix shows the scatter and the lower triangular matrix shows the correlation between them (proper explanation is given in the [Seismicity of the Study Area and Data](#) section). The color version of this figure is available only in the electronic edition.

coefficients corresponding to the ground-motion parameter, the moment magnitude, the hypocentral distance, and the average shear-wave velocity at a depth of 30 m. The units corresponding to PGA, $PSA_{0.3\text{ s}}$, $PSA_{1.0\text{ s}}$, $PSA_{2.0\text{ s}}$, and $PSA_{3.0\text{ s}}$ are cm/s^2 and cm/s for the PGV. In the following, equations 1–3 will be denoted as models 1–3, respectively.

In this present study, an orthogonal regression, which is also known as total least square or Deming orthogonal regression (Deming, 1943; Markovsky and Van Huffel, 2007), has been used to derive the regression coefficients for relating the MMI and the ground-motion parameters for two reasons. First, the ordinary least-squares method minimizes the sum of the square of the vertical distance, whereas the orthogonal regression method minimizes the sum of the squared orthogonal distance from the data point to the fitting line. Second, the ordinary least-squares regression analysis assumes that the independent variable is measured without error, whereas the measure of the dependent variable is affected by errors. Orthogonal regression analysis accommodates this uncertainty in both the dependent and independent variables. Asymmetry arises in the ordinary least-squares analysis, because both the dependent and independent variables are not treated symmetrically. To overcome this, Deming orthogonal regression looks for a minimal correction in both the dependent and the independent variables to give a corrected system of equations (Markovsky and Van Huffel, 2007).

Orthogonal regression is a solution to an overdetermined system of equations $AX \approx B$, in which $A \in \mathbb{R}^{m \times n}$ and $B \in \mathbb{R}^{m \times d}$ are the given data and $X \in \mathbb{R}^{n \times d}$ is unknown. Therefore, orthogonal regression is the generalization of the

least-squares approximation method when both A and B are perturbed. Orthogonal regression looks to minimize the correction, that is, ΔA and ΔB in the given data A and B , and to make the corrected system of equations $\hat{A}X = \hat{B}$, in which $\hat{A} := A + \Delta A$ and $\hat{B} := B + \Delta B$ are solvable, that is, $\{\hat{X}, \Delta A, \Delta B\} := \operatorname{argmin}_{X, \Delta A, \Delta B} \|\Delta A \Delta B\|_F$ subject to $(A + \Delta A)X = B + \Delta B$. This is the solution of the optimal corrected systems of equations and is the maximum-likelihood estimator in the errors-in-variable models (Markovsky and Van Huffel, 2007). When $A = \bar{A} + \tilde{A}$, $B = \bar{B} + \tilde{B}$, exists an $\bar{X} \in \mathbb{R}^{n \times d}$ exists, such that $\bar{A}\bar{X} = \bar{B}$ under the assumption that $\operatorname{vec}([\hat{A} \hat{B}])$ is a zero mean, normally distributed random vector with a covariance matrix that is a multiple of identity. The errors in the variable model \bar{A} and \bar{B} are the true data; \bar{X} is the true value of the parameter X ; and \tilde{A} and \tilde{B} consist of measurement error. Orthogonal regression reduces the sum of the squared residuals for both the dependent and the independent variables simultaneously and requires the error for both independent and dependent variables. The formulation regarding multivariate regression is given in de Groen (1996), which is used in this study to derive the regression coefficients for relating the MMI and the ground-motion parameters. From a statistical point of view, the orthogonal regression method removes bias by deducting the error covariance matrix from the data covariance matrix. It also weights the residuals by multiplying them with the inverse of the corresponding error covariance matrix to derive a consistent estimate.

Table 2

Mean (μ) and Standard Deviation (σ) for log (PGA), log (PGV), log (PSA [0.3 s]), log (PSA [1.0 s]), log (PSA [2.0 s]), and log (PSA [3.0 s]) along with Number of Observation

MMI	log (PGA) (cm/s ²)		log (PGV) (cm/s)		log(PSA _{0.3 s}) (cm/s ²)		log(PSA _{1.0 s}) (cm/s ²)		log(PSA _{2.0 s}) (cm/s ²)		log(PSA _{3.0 s}) (cm/s ²)		Number of Observations
	μ	σ	μ	σ	μ	σ	μ	σ	μ	σ	μ	σ	
I	0.053	0.913	-1.363	1.075	-0.167	1.577	-0.668	1.222	-0.716	1.004	-1.043	0.802	6
II	0.659	0.455	0.367	0.476	1.032	0.626	0.258	0.421	0.044	0.390	-0.668	0.501	20
III	1.059	0.389	0.215	0.933	1.413	0.526	0.798	0.528	0.543	0.530	-0.061	0.674	42
IV	1.182	0.487	0.351	0.883	1.665	0.489	0.884	0.599	0.713	0.639	0.141	0.918	62
V	1.832	0.346	0.546	0.388	2.123	0.505	1.470	0.657	1.344	0.578	1.082	0.650	33
VI	1.868	0.254	0.781	0.298	2.246	0.334	1.783	0.346	1.612	0.214	1.141	0.486	16
VII	2.217	0.285	1.077	0.911	2.250	0.707	1.777	0.877	1.634	0.943	1.126	0.994	8
VIII	2.445	0.126	1.299	0.592	2.462	1.487	1.976	0.675	1.860	0.320	1.106	1.200	3
IX	2.207	-	2.031	-	2.646	-	2.451	-	2.411	-	2.366	-	1

To verify the regressed models further, several statistical tests were performed. An ANOVA was carried using the *F*-test to verify the regional dependency of the coefficients. An ANOVA is the hypothesis test that is suitable for inferring whether the mean of the continuous independent variables (two or more) are equal. It compares the probability associated with the null hypothesis (*p*-value) that the means are equal. In this study, the ANOVA is performed between the observed and calculated MMI values using different ground-motion parameters. The *F*-test is also performed, however, to check whether the regression model fits the data well. In a linear model such as $Y_j = \alpha + \beta_1 X_{1j} + \dots + \beta_n X_{nj}$, to conduct the *F*-test, *F* is calculated according to:

$$F = \frac{(SSR - SSE)/k}{SSE/(n - k)} = \frac{R^2/k}{(1 - R^2)/(n - k + 1)}, \quad (4)$$

in which SSR is the sum of the squared residuals and SSE is the sum of the squared error. The larger the *F*-statistic, the more useful the model. A residual analysis was also performed to verify whether the residuals are normally distributed around a zero mean with a constant variance and are uncorrelated. First, the *t*-test was performed to verify the distribution of the residuals around zero. A positive test confirms that the models fit the data. Second, the DW-test was performed to validate the statistical significance of the regression. This test is used to detect the autocorrelation, that is, the dependency of the residuals. The test statistic is defined as

$$d = \frac{\sum_{i=2}^n (e_i - e_{i-1})^2}{\sum_{i=1}^n e_i^2}, \quad (5)$$

in which $e_i = y_i - \hat{y}_i$, and y_i and \hat{y}_i are the observed and predicted values of the response variable for individual *i*, respectively. If $d < 2$, there is a positive serial correlation, and if $d > 2$, there is a negative serial correlation. Furthermore, to validate the variance of the residuals, the BP-test was carried out. This test is also dependent on the goodness of fit. Because the regression equation has been developed between the MMI and the ground-motion parameters with or without shear-wave velocity, the entire test was done to validate that the statistical

inference of the regression coefficients corresponds to their respective parameters.

Relationship between the MMI and the Ground-Motion Parameters

The simple regression relationship was derived between the MMI as the dependent variable and the ground-motion parameters such as the PGA, the PGV, and the PSA as the independent variables. To address the uneven distribution of the ground-motion parameters corresponding to a single macroseismic intensity, the mean of the PGA, the PGV, and the PSA was taken at each MMI level (I–IX). The same approach has been adopted by other researchers (Kaka and Atkinson, 2004; Tselentis and Danciu, 2008; Bilal and Askan, 2014). Table 2 shows the mean and standard deviations corresponding to log (PGA), log (PGV), log(PSA_{0.3 s}), log(PSA_{1.0 s}), log(PSA_{2.0 s}), and log(PSA_{3.0 s}). Table 3 presents the results of the orthogonal regression analysis between the MMI and log (PGA), log (PGV), log(PSA_{0.3 s}), log(PSA_{1.0 s}), log(PSA_{2.0 s}), and log(PSA_{3.0 s}), with units of cm/s² for the PGA and the PSA and cm/s for the PGV, respectively, using model 1. Along with the regression coefficient, the coefficient of determination (*R*²), and the sum of squared residuals is also presented in Table 3. Based on the *R*² and the sum of squared residuals, it can be concluded that the MMI is regressed well with the log of the average of the ground-motion parameters. The macroseismic intensity, however, would be affected by far-field and near-field earthquakes, which in turn depend upon the hypocentral distance, the moment magnitude, and the site upper crustal amplification. Therefore, in the next section, improved regression relationships were developed by incorporating hypocentral distance, moment magnitude, and the V_{S30} values.

Relationship between MMI and Recorded Ground-Motion Parameters

The relationship between the ground-motion parameters and the MMI can be refined further by incorporating moment magnitude (M_w), hypocentral distance (*R*), and average

Table 3
Regression Coefficients for Simple Empirical Regression between MMI and Ground-Motion Parameter Using Model 1

Regression Equation	Regression Coefficient		R^2	SSR	σ
	a (sa)	b (sb)			
MMI = $a + b$ PGA	0.142 (± 0.68)	3.233 (± 0.37)	0.92	5.111	0.52
MMI = $a + b$ PGV	3.422 (± 0.48)	2.679 (± 0.46)	0.83	7.378	0.55
MMI = $a + b$ PSA _{0.3 s} + σ	0.045 (± 0.46)	2.846 (± 0.46)	0.85	6.371	0.56
MMI = $a + b$ PSA _{1.0 s} + σ	1.765 (± 0.28)	2.713 (± 0.28)	0.93	4.412	0.58
MMI = $a + b$ PSA _{2.0 s} + σ	2.713 (± 0.24)	2.152 (± 0.24)	0.95	4.425	0.62
MMI = $a + b$ PSA _{3.0 s} + σ	3.589 (± 0.28)	2.447 (± 0.28)	0.91	5.354	0.65

R^2 , coefficient of determination; SSR, sum of square of residual; σ , standard error of the equation; sa and sb , standard error in a and b .

Table 4
Regression Coefficients for Empirical Regression between MMI, Ground-Motion Parameter, Hypocentral Distance (R), and Moment Magnitude (M_w)

Regression Equation	Regression Coefficient				R^2	σ
	a (sa)	b (sb)	c (sc)	d (sd)		
MMI = $a + b \log(\text{PGA}) + cM_w + d \log R + \sigma$	2.374 (± 0.66)	0.702 (± 0.14)	0.734 (± 0.11)	-1.664 (± 0.21)	0.67	0.56
MMI = $a + b \log(\text{PGV}) + cM_w + d \log R + \sigma$	1.636 (± 0.75)	0.264 (± 0.07)	1.041 (± 0.09)	-1.821 (± 0.20)	0.58	0.57
MMI = $a + b \log \text{PSA}_{0.3 s} + cM_w + d \log R + \sigma$	1.068 (± 0.78)	0.223 (± 0.13)	1.017 (± 0.12)	-1.616 (± 0.26)	0.56	0.56
MMI = $a + b \log \text{PSA}_{1.0 s} + cM_w + d \log R + \sigma$	1.646 (± 0.82)	0.215 (± 0.14)	0.992 (± 0.99)	-1.732 (± 0.25)	0.55	0.55
MMI = $a + b \log \text{PSA}_{2.0 s} + cM_w + d \log R + \sigma$	1.735 (± 0.89)	0.249 (± 0.16)	0.945 (± 0.16)	-1.648 (± 0.28)	0.54	0.56
MMI = $a + b \log \text{PSA}_{3.0 s} + cM_w + d \log R + \sigma$	1.495 (± 0.88)	0.006 (± 0.13)	1.111 (± 0.15)	-1.889 (± 0.26)	0.54	0.54

shear-wave velocity up to a depth of 30 m (V_{S30}). The other important aspect for developing these equations is to predict the ground-motion amplitude at a site with known M_w and R corresponding to a particular MMI value for the regions where recording stations are not available in abundance. The refined empirical relationship between the MMI and the ground-motion parameters is developed by incorporating M_w and R and by incorporating the calculated V_{S30} value. The regression coefficients derived using orthogonal regression for model 2, along with the standard error and coefficient of determination (R^2), are given in Table 4. This analysis shows that the standard error in the determination of the MMI would be ± 0.55 to ± 0.57 . It can also be noted from the statistical analysis of the present database that, when using any of the ground-motion parameters with the presently developed regression equations, the standard error is almost constant in determining the MMI value. It can be concluded, therefore, that the building damage due to ground shaking can be accounted for by any of the PGA, the PGV, or the PSA models and that these empirical models will predict the MMI value within a margin of error of ± 0.56 for the Himalayan region. The $Q-Q$ plot was also used to check whether the assumed probability distribution of the residuals is valid. The $Q-Q$ plot presents the quintile of the variable distribution with the variable in the quintile of the test distribution. Figure 3a-f shows the $Q-Q$ plots for the residuals between MMI and PGA, MMI and PGV, MMI and PSA_{0.3 s}, MMI and PSA_{1.0 s}, MMI and PSA_{2.0 s}, and MMI and PSA_{3.0 s},

respectively, by including hypocentral distance and moment magnitude as independent variables in the relationship. It can be concluded from Figure 3 that the residuals from all the relationships are normally distributed. This confirms the validity of the regression coefficients derived using orthogonal regression in one aspect.

Because intensity is also a function of a site effect that can be represented widely in terms of V_{S30} , V_{S30} could be a potential independent variable for determining the macroseismic intensity for any site. The shear-wave velocity at different stations was therefore calculated using the empirical relationship developed by Ghofrani and Atkinson (2014) by considering the peak frequency and peak amplitude from HVSR spectrum at different seismic station sites. To derive the V_{S30} using this empirical relationship, only the sites having a peak frequency greater than or equal to 1 Hz were considered, according to Ghofrani and Atkinson (2014). It was found that all these sites lie within site classes D and E, except for the 10 sites that lie in site class A or B according to the National Earthquake Reduction Program classification. The final derived model for evaluating the MMI considering V_{S30} has a functional form similar to model 3 above. The regression coefficients, the standard errors, and the coefficients of determination are given in Table 5 by incorporating the hypocentral distance, the magnitude, and the shear-wave velocity as independent variables in the relationship. Figure 4a-f shows the $Q-Q$ plot of the residuals between MMI and PGA, MMI and PGV, MMI and PSA_{0.3 s}, MMI and PSA_{1.0 s}, MMI and PSA_{2.0 s}, and MMI and PSA_{3.0 s}, respectively. The $Q-Q$ plot confirms the validity of

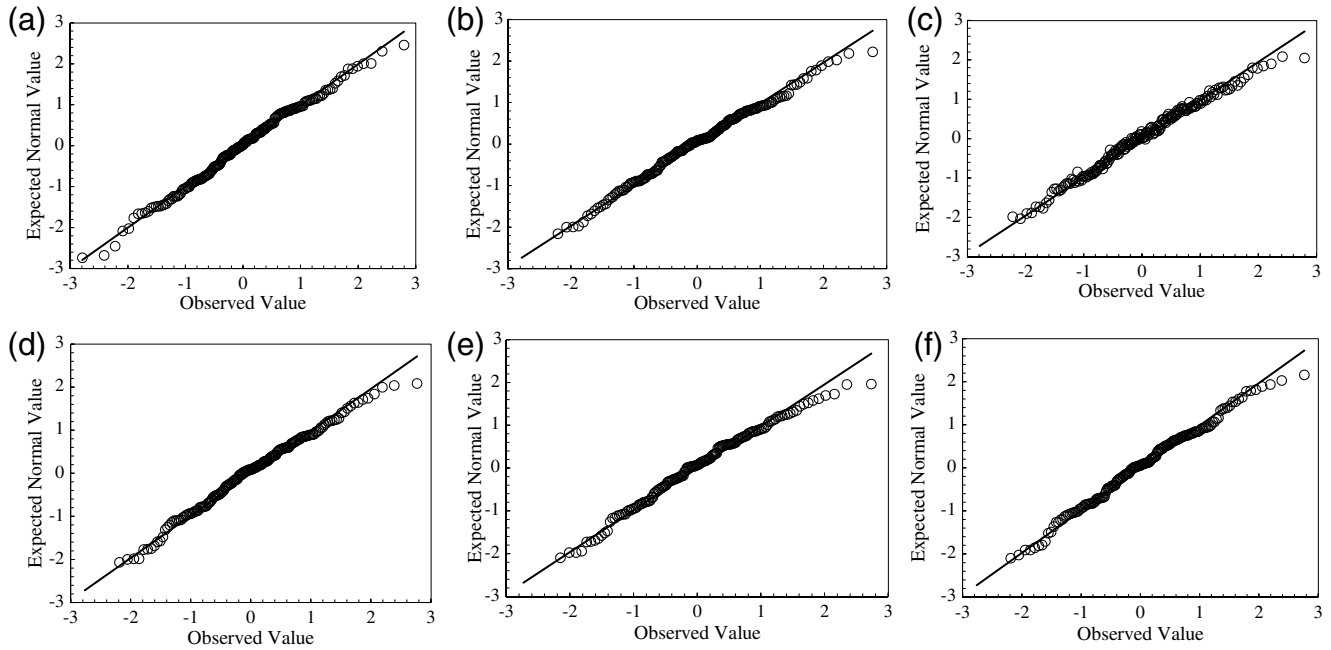


Figure 3. Probability plots in terms of quintile–quintile ($Q-Q$) plots for the (a) MMI versus PGA, (b) MMI versus PGV, (c) MMI versus $PSA_{0.3s}$, (d) MMI versus $PSA_{1.0s}$, (e) MMI versus $PSA_{2.0s}$, and (f) MMI versus $PSA_{3.0s}$ residuals for model 1.

the regression relationships, because the residuals from all the relationships are normally distributed with zero mean and σ . In comparison with Figure 3, it can be seen that there is little change in the distribution of the residuals, although the distribution follows a good trend when the site-effect factor is included. It can be seen from Tables 4 and 5 that the coefficients of determination when V_{S30} is included as one of the independent variables are less compared to the MMI computed using M_w and R . Furthermore, the standard error in determining the MMI value is the same whether V_{S30} is incorporated as an independent variable or not.

Residual plots were compared for all three regression models developed in this study for determining the MMI. The residuals, that is, $MMI_{obs} - MMI_{pre}$, were calculated,

in which MMI_{obs} and MMI_{pre} are the observed and predicted values of the MMI, respectively. The MMI_{pre} was calculated using the presently derived relationship between the MMI and the ground-motion parameters (i.e., models 2 and 3). The residuals calculated using these two models were plotted against the moment magnitude and the hypocentral distance. Figures 5a–f and 6a–f show the variation of the residuals with respect to hypocentral distance and magnitude, corresponding to models 2 and 3. It can be seen from Figures 5 and 6 that the residual difference is greater when calculating MMI as dependent on the PGA using model 2, compared to using model 3. This finding may be related to the site effect and type structure in the region, as this effect is less in case of PGV for a distance of less than 300 km. In contrast, most of

Table 5

Regression Coefficients for Empirical Regression between MMI, Ground-Motion Parameter, Hypocentral Distance (R), Moment Magnitude (M_w), and Shear-Wave Velocity at 30 m Depth (V_{S30})

Regression Equation	Regression Coefficient					R^2	σ
	a (sa)	b (sb)	c (sc)	d (sd)	e (se)		
$MMI = a + b \log(PGA) + cM_w + d \log R + e \log V_{S30} + \sigma$	2.132 (± 2.53)	0.266 (± 0.15)	0.981 (± 0.12)	-1.671 (± 0.23)	-0.256 (± 0.80)	0.62	0.53
$MMI = a + b \log(PGV) + cM_w + d \log R + e \log V_{S30} + \sigma$	1.992 (± 2.13)	0.239 (± 0.08)	1.061 (± 0.10)	-1.825 (± 0.28)	-0.167 (± 0.76)	0.57	0.52
$MMI = a + b \log PSA_{0.3s} + cM_w + d \log R + e \log V_{S30} + \sigma$	1.383 (± 1.01)	0.300 (± 0.07)	0.961 (± 0.13)	-1.517 (± 0.27)	-0.113 (± 0.57)	0.56	0.51
$MMI = a + b \log PSA_{1.0s} + cM_w + d \log R + e \log V_{S30} + \sigma$	2.263 (± 3.18)	0.281 (± 0.15)	0.932 (± 0.15)	-1.673 (± 0.28)	-0.157 (± 0.98)	0.54	0.51
$MMI = a + b \log PSA_{2.0s} + cM_w + d \log R + e \log V_{S30} + \sigma$	1.916 (± 3.21)	0.275 (± 0.17)	0.925 (± 0.16)	-1.635 (± 0.29)	-0.168 (± 0.99)	0.54	0.51
$MMI = a + b \log PSA_{3.0s} + cM_w + d \log R + e \log V_{S30} + \sigma$	1.820 (± 3.24)	-0.169 (± 0.15)	1.141 (± 0.17)	-1.901 (± 0.30)	-0.013 (± 1.02)	0.52	0.53

R^2 , coefficient of determination; σ , standard error of the equation; sa , sb , sc , sd , and se , standard error in a , b , c , d , and e , respectively.

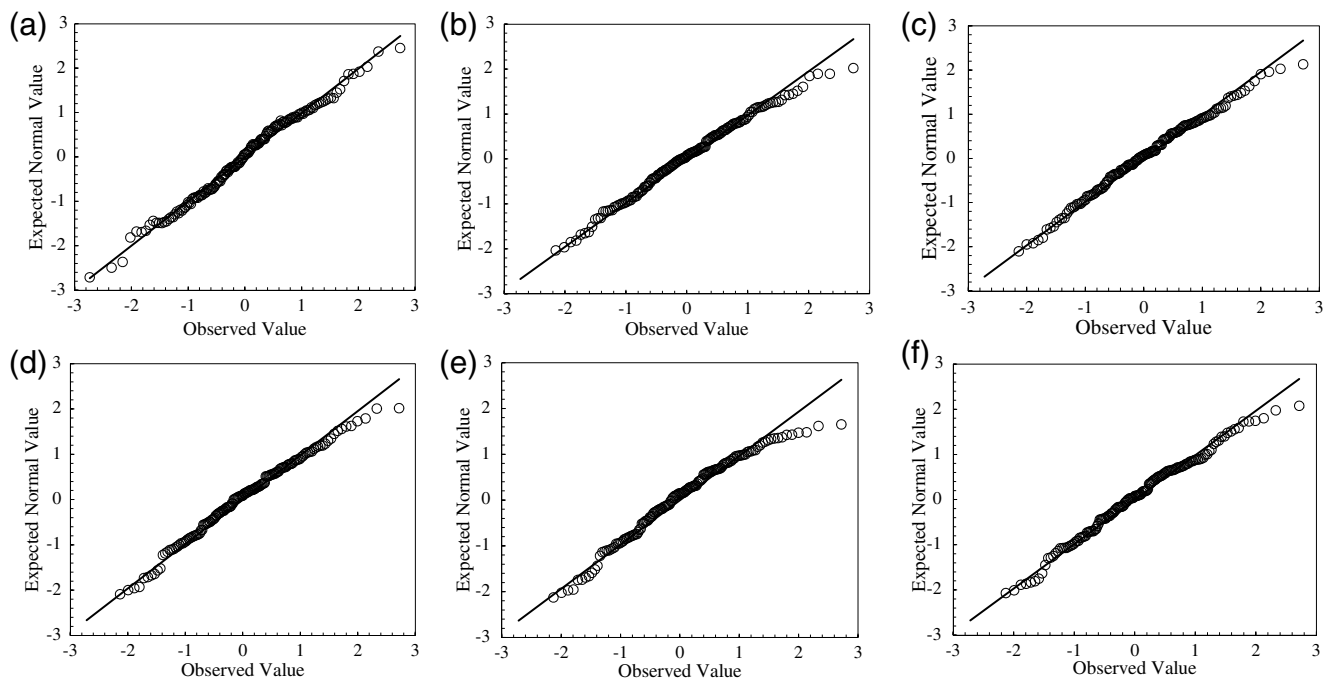


Figure 4. Probability plots in terms of $Q-Q$ plots for the (a) MMI versus PGA, (b) MMI versus PGV, (c) MMI versus $PSA_{0.3\text{ s}}$, (d) MMI versus $PSA_{1.0\text{ s}}$, (e) MMI versus $PSA_{2.0\text{ s}}$, and (f) MMI versus $PSA_{3.0\text{ s}}$ residuals for model 2.

the structures in the study area are nonductile and low-rise structures that have short time periods (i.e., time periods of less than 0.3 s reference), even though the site effect is seen in the PSA value at long periods. This observation concurs with that of Prasad *et al.* (2009) that most of the buildings in the Himalayan region are constructed of random rubble masonry, masonry walls constructed using rectangular units, and low-rise-framed structures. These types of structures tend to collapse or experience extensive damage when the amplification is large and at a high frequency. Jain *et al.* (1992) reported that buildings with random rubble masonry suffered extensive damage in the 1991 Garhwal earthquake. Further, diagonal cracks and damage at beam-column joints and in the connections between slabs and masonry walls were observed in low-rise-reinforced concrete structures. Similarly, Jain *et al.* (1999) reported an intensity of VII near a river terrace, which was at an aerial distance of about 20 km from the epicenter where most dwellings collapsed due to site amplification. Parameswaran *et al.* (2015) reported that most of the structures that were damaged during the 2015 Gorkha (Nepal) earthquake were nonengineered brick houses and multistoried apartment complexes that probably collapsed due to a lack of structural integrity. Other researchers (Jain *et al.*, 1999; Parameswaran *et al.*, 2015) also report that, while buildings were often initially planned to be just a few stories, in time more floors were added without strengthening the foundations, and that this is one of the major causes for building collapse during earthquakes.

When the hypocentral distance was greater than 300 km, the effect of velocity seems to be more pronounced. This finding may be because of the far-field effect, which is reflected in

the observed MMI value. Therefore, to determine the MMI using the PGA value, model 3 should be used for hypocentral distances greater than 300 km to incorporate the far-field site effect. The same effect is seen in determining the MMI using PGV, $PSA_{0.3\text{ s}}$, $PSA_{1.0\text{ s}}$, $PSA_{2.0\text{ s}}$, and $PSA_{3.0\text{ s}}$ using models 2 and 3, however. It can be concluded from Figures 5 and 6 that the MMI can be determined using either of the ground-motion parameters, but the site effect (V_{S30}) needs to be considered.

This study shows that incorporation of the site-specific shear-wave velocity will help to account for site and building effects in the prediction of the MMI considering PGA. In many cases, however, the shear-wave velocity profile of a region is not available, so this study attempts to counterbalance the site effect for such sites, considering the relationship between MMI_{obs} and MMI_{pre} for models 2 and 3 (taking X as PGA). The relationship between the observed and predicted MMI using models 2 and 3 (taking X as PGA) is given in Figure 7a. From the derived relationship, it can be seen that the predicted MMI using model 3 is 0.137 more than the MMI calculated using model 2, that is, $MMI_{\text{pre}}(\text{model 3}) = MMI_{\text{pre}}(\text{model 2}) + 0.197$. Therefore, equation (6), to predict MMI with the site effect but without V_{S30} , is

$$MMI_{\text{mod}} = 2.571 + 0.702 \log(\text{PGA}) + 0.734M_w - 1.664 \log(R) + \sigma, \quad (6)$$

in which MMI_{mod} is the modified MMI. MMI_{mod} is included as a new term to remove the confusion between the MMI calculated using model 2 or in the modified relationship. To check the validity of the MMI calculated using the modified relationship or in model 3, the plot between the observed

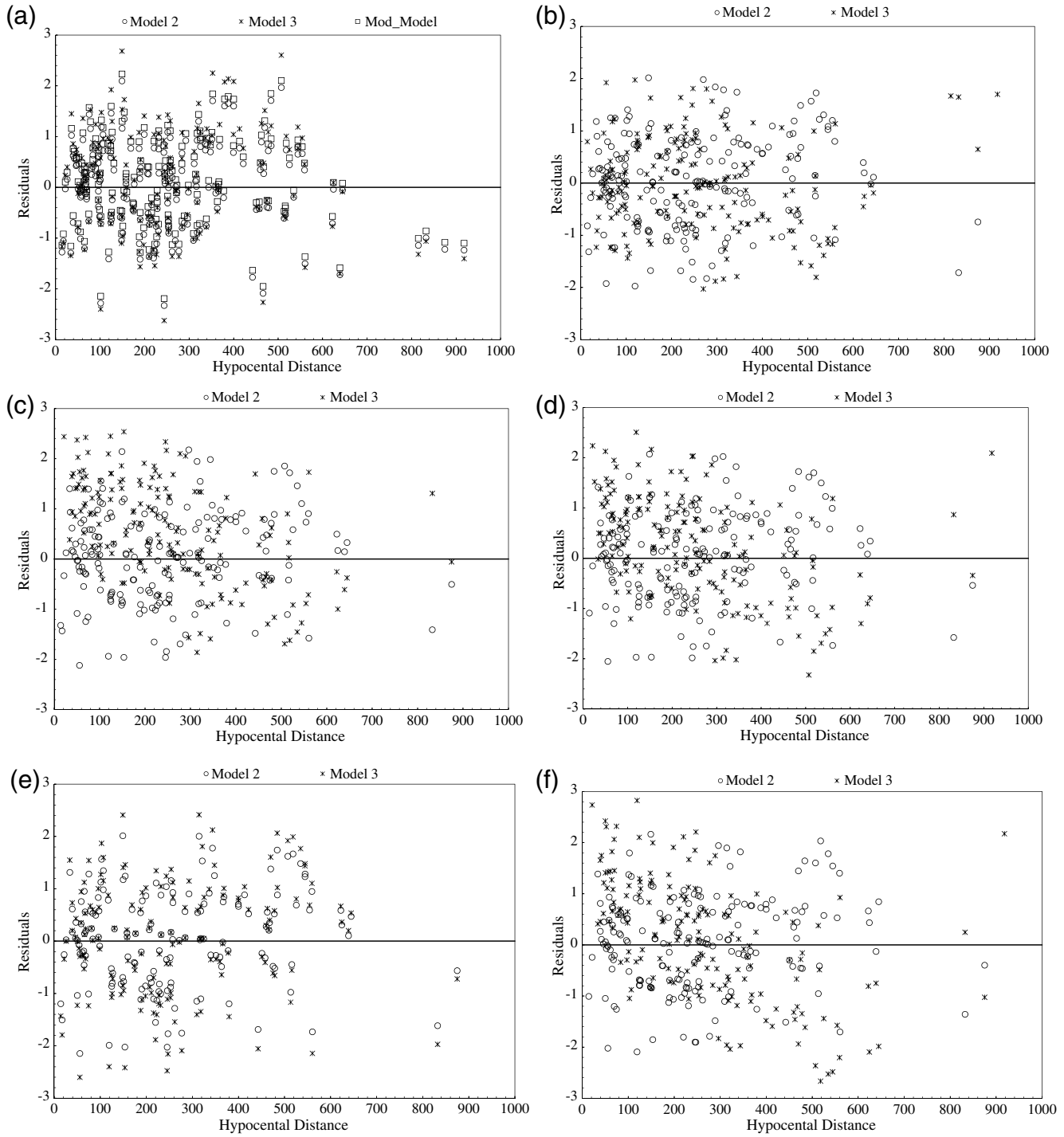


Figure 5. Residuals of (a) MMI versus PGA, (b) MMI versus PGV, (c) MMI versus $PSA_{0.3s}$, (d) MMI versus $PSA_{1.0s}$, (e) MMI versus $PSA_{2.0s}$, and (f) MMI versus $PSA_{3.0s}$ relationships derived using models 2 and 3 as a function of the hypocentral distance (km).

MMI and MMI calculated using model 3 (taking X as PGA) and MMI_{mod} is given in Figure 7b. It can be seen from Figure 7b that both trend lines almost coincide. Therefore, for the regions where V_{S30} is not available, the MMI_{mod} equation can be used as an alternative. Further, it can be clearly seen from Figures 5a and 6a that the residual in MMI calculated using model 3 and in the modified model for the PGA also almost coincide. This particular equation, however, is only valid for the Himalayan

region, and the standard error associated with the modified model is ± 0.53 . Most of the sites considered in this study are in site classes B, C, and D, but the same procedure can be followed if sufficient data are available for site classes A and E. From Figures 5a, 6a, and 7b, it can be seen that by incorporating an additional constant factor for the site and building effect in the correlations, the predicted MMI value can be effectively improved.

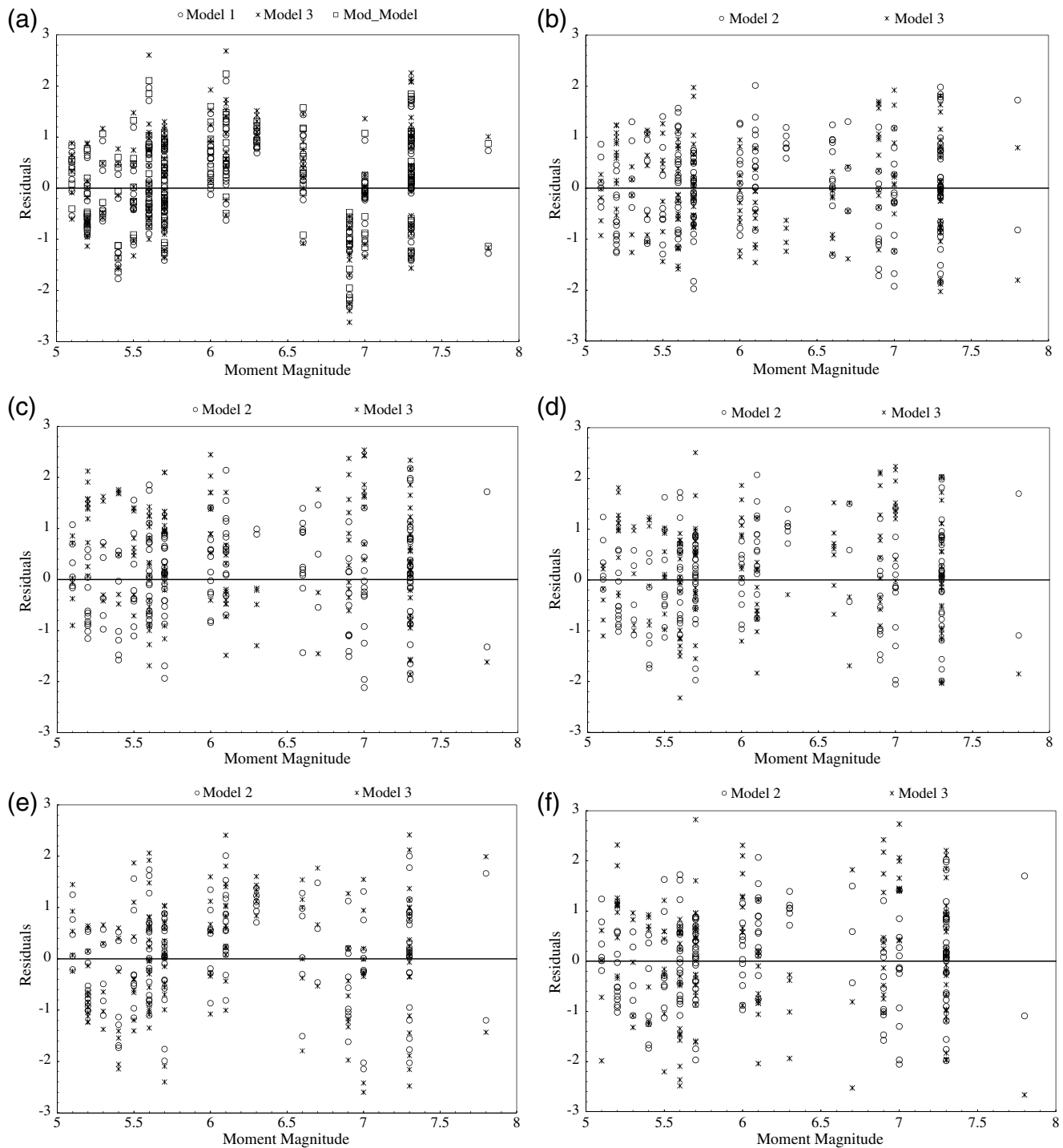


Figure 6. Residuals of (a) MMI versus PGA, (b) MMI versus PGV, (c) MMI versus $PSA_{0.3s}$, (d) MMI versus $PSA_{1.0s}$, (e) MMI versus $PSA_{2.0s}$, and (f) MMI versus $PSA_{3.0s}$ relationships derived using models 2 and 3 as a function of moment magnitude (km).

Verifying Model Assumptions

The regression models developed were further verified using various tests: the F -test, the t -test, the DW-test, and the BP-test. The applicability of these tests has been already explained by [Caprio et al. \(2015\)](#). These tests were performed

in this research to verify the implicit assumption that the residuals are normally distributed around zero with a constant variance.

1. An ANOVA was performed to verify the regional dependency as a significant variable by assigning a dummy

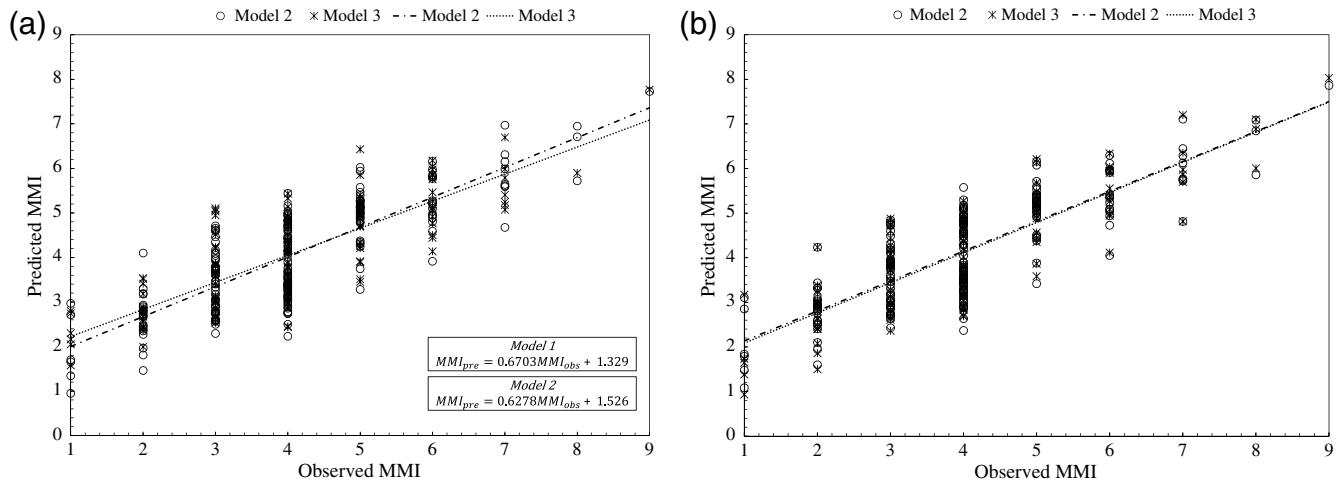


Figure 7. Modifying the MMI versus PGA relationship to counterbalance the site-effect: (a) relationship between the MMI observed and the MMI predicted using models 2 and 3 (taking X as PGA), and (b) validation of the calculated MMI modified by plotting the observed MMI and the calculated MMI using model 3 (taking X as PGA) and MMI_{mod} .

variable to these regression equations. This passed the hypothesis with a p -value equal to 3.2×10^{-8} .

2. An F -test was conducted using the SSR ANOVA and SSE. The F -value was derived from this. The F -value corresponds to the three models as shown in Table 6. It can be seen from Table 6 that the variance between the predicted and the observed MMI is equal at the 95% significance level. The same can also be seen based on the p -value.
3. The t -test verifies the distribution of residuals around zero, and the positive result confirms that the regression model developed in this study fits the data.
4. The DW-test was conducted, and, based on the information in Table 6, it can be seen that the residuals are pos-

itively correlated, because the d value is less than two in each case.

5. Based on the p -value calculated after conducting the BP-test, the regression models derived in this study accept the null hypothesis of homoscedasticity and reject heteroscedasticity.

Based on these tests, it can be concluded that the models developed in this study have passed all the tests at the 95% confidence level. It can be stated that the regression coefficients derived in this study using different models are representative of the data, and the residuals also perform well.

Table 6
Different Values of the Statistics Correspond to Different Tests along with p -Values That Correspond to Three Models Used in This Study

Models	Correlations	F -Test		t -Test	DW-Test	BP-Test
		F -Value	p -Value			p -Value
Model 1	MMI-PGA	96.882	0.0036	1	1.259	0.12
	MMI-PGV	43.941	0.0056	1	1.325	0.10
	MMI-PSA _{0.3s}	51.000	0.0068	1	1.389	0.10
	MMI-PSA _{1.0s}	119.571	0.0057	1	1.426	0.14
	MMI-PSA _{2.0s}	82.358	0.0054	1	1.452	0.11
Model 2	MMI-PSA _{3.0s}	91.000	0.0055	1	1.467	0.14
	MMI-PGA	127.909	0.0006	1	1.257	0.10
	MMI-PGV	87.000	0.0005	1	1.328	0.10
	MMI-PSA _{0.3s}	77.636	0.0002	1	0.841	0.10
	MMI-PSA _{1.0s}	71.703	0.0078	1	0.815	0.12
Model 3	MMI-PSA _{2.0s}	63.875	0.0045	1	0.726	0.10
	MMI-PSA _{3.0s}	67.695	0.0028	1	0.712	0.13
	MMI-PGA	64.447	0.0251	1	1.663	0.13
	MMI-PGV	52.029	0.0452	1	1.107	0.10
	MMI-PSA _{0.3s}	48.363	0.0655	1	1.737	0.10
	MMI-PSA _{1.0s}	44.021	0.0647	1	1.872	0.10
	MMI-PSA _{2.0s}	45.401	0.0628	1	1.722	0.12
	MMI-PSA _{3.0s}	40.354	0.0545	1	1.858	0.13

DW-test, Durbin-Watson test; BP-test, Breusch-Pagan test.

Table 7

Empirical Relationship between MMI and Ground-Motion Parameter Defined as Model 1 from the Previous and Present Study along with θ Value for Comparison of Models

Model 1	Reference Study	Proposed Equation	Data Source	θ Value	
MMI-PGA	Wald <i>et al.</i> (1999)	$MMI = -1.66 + 3.66 \log PGA$	California	1.285	
	Arioglu <i>et al.</i> (2001)	$MMI = -1.078 + 1.748 \log PGA$	Turkey	1.416	
	Atkinson and Kaka (2007)	$MMI = 2.65 + 1.39 \log PGA, \log PGA \leq 1.69$ $MMI = -1.91 + 4.09 \log PGA, \log PGA > 1.69$	Central United States and California	1.275	
	Tselentis and Danciu (2008)	$MMI = -0.946 + 3.563 \log PGA$	Greece	1.205	
	Faenza and Michelini (2010)	$MMI = 1.68 + 2.58 \log PGA$	Italy	1.228	
	Worden <i>et al.</i> (2012)	$MMI = 1.78 + 1.55 \log PGA, \log PGA \leq 1.57$ $MMI = 3.78 + 1.47 \log PGA, \log PGA > 1.57$	California	1.189	
	Bilal and Askan (2014)	$MMI = 0.132 + 3.884 \log PGA$	Turkey	1.158	
	Caprio <i>et al.</i> (2015)	$MMI = 4.424 + 1.589 \log PGA, \log PGA \leq 0.3$ $MMI = 4.018 + 2.671 \log PGA, \log PGA > 0.3$	Worldwide	1.305	
	This study	$MMI = 0.1417 + 3.2335 \log PGA$	Himalayan region	1.121	
	MMI-PGV	Wald <i>et al.</i> (1999)	$MMI = 2.35 + 3.47 \log PGV$	California	1.284
		Kaka and Atkinson (2004)	$MMI = 3.96 + 1.79 \log PGV$	East North America	1.328
		Atkinson and Kaka (2007)	$MMI = 4.37 + 1.32 \log PGV, \log PGV \leq 0.48$ $MMI = 3.54 + 3.03 \log PGV, \log PGV > 0.48$	Central United States and California	1.405
		Tselentis and Danciu (2008)	$MMI = 3.30 + 3.358 \log PGV$	Greece	1.394
		Faenza and Michelini (2010)	$MMI = 5.11 + 2.35 \log PGV$	Italy	1.309
Worden <i>et al.</i> (2012)		$MMI = 3.78 + 1.47 \log PGV, \log PGV \leq 0.53$ $MMI = 2.89 + 3.16 \log PGV, \log PGV > 0.53$	California	1.258	
Bilal and Askan (2014)		$MMI = 2.673 + 4.34 \log PGV$	Turkey	1.264	
Caprio <i>et al.</i> (2015)		$MMI = 2.27 + 1.647 \log PGV, \log PGV \leq 1.6$ $MMI = -1.361 + 3.822 \log PGV, \log PGV > 1.6$	Worldwide	1.268	
This study		$MMI = 3.422 + 2.679 \log PGV$	Himalayan region	1.252	
MMI-PSA _{0.3 s}		Worden <i>et al.</i> (2012)	$MMI = 1.26 + 1.69 \log PSA_{0.3 s}, \log PSA_{0.3 s} \leq 2.21$ $MMI = -4.15 + 4.14 \log PSA_{0.3 s}, \log PSA_{0.3 s} > 2.21$	California	1.254
		Bilal and Askan (2014)	$MMI = -0.247 + 3.404 \log PSA_{0.3 s}$	Turkey	1.234
		This study	$MMI = 0.045 + 2.846 \log PSA_{0.3 s}$	Himalayan region	1.208
MMI-PSA _{1.0 s}		Atkinson and Sonley (2000)	$MMI = -2.0 + 4 \log PSA_{1.0 s}$	California	1.305
		Worden <i>et al.</i> (2012)	$MMI = 2.5 + 1.51 \log PSA_{1.0 s}, \log PSA_{1.0 s} \leq 1.65$ $MMI = 0.2 + 2.9 \log PSA_{1.0 s}, \log PSA_{1.0 s} > 1.65$	California	1.284
	Bilal and Askan (2014)	$MMI = -0.934 + 4.119 \log PSA_{1.0 s}$	Turkey	1.257	
	This study	$MMI = 1.765 + 2.713 \log PSA_{1.0 s}$	Himalayan region	1.212	
MMI-PSA _{2.0 s}	Bilal and Askan (2014)	$MMI = -0.313 + 4.453 \log PSA_{2.0 s}$	Turkey	1.295	
	This study	$MMI = 2.713 + 2.152 \log PSA_{2.0 s}$	Himalayan region	1.212	
MMI-PSA _{3.0 s}	Worden <i>et al.</i> (2012)	$MMI = 3.81 + 1.71 \log PSA_{3.0 s}, \log PSA_{3.0 s} \leq 0.99$ $MMI = 1.99 + 3.01 \log PSA_{3.0 s}, \log PSA_{3.0 s} > 0.99$	California	1.310	
	This study	$MMI = 3.589 + 2.447 \log PSA_{3.0 s}$	Himalayan region	1.272	

Comparison of the Present Relationship with Previous Studies

The empirical relationship between the MMI and the ground-motion parameters developed in this study (described by the three models) were compared with similar relationships developed for different regions worldwide. A comparison between these models is a good indicator of the probable variation in the empirical relationships from one region to another. The relationship between the MMI and the PGA (using model 1) derived in this study was compared with the similar relationships developed in the following studies: Wald *et al.* (1999), Arioglu *et al.* (2001), Tselentis and Danciu (2008), Faenza and Michelini (2010), Nath and Thingbaijam (2011), Worden *et al.* (2012), Bilal and Askan (2014), and Caprio *et al.* (2015). Similarly, the relationship between the MMI and the PGV was compared

with the studies carried out by Wald *et al.* (1999), Kaka and Atkinson (2004), Tselentis and Danciu (2008), Faenza and Michelini (2010), Worden *et al.* (2012), Bilal and Askan (2014), and Caprio *et al.* (2015). The relationships between the MMI and the PGA and the MMI and the PGV developed using model 2 was compared with Atkinson and Kaka (2007), Tselentis and Danciu (2008), Worden *et al.* (2012), and Bilal and Askan (2014). The relationship between the MMI and the PSA at 0.3, 1.0, 2.0, and 3.0 s developed using models 2 and 3 was compared with Atkinson and Sonley (2000), Worden *et al.* (2012), and Bilal and Askan (2014). The equations derived by these various researchers for comparison with this study are given in Table 6. Tables 7 and 8 provide the empirical relationships derived, based on models 1 and 2, respectively. Figure 8a–c corresponds to the comparison of the empirical relationship derived from model 1 with the existing equations given in Table 7. The database

Table 8

Empirical Relationship between MMI and Ground-Motion Parameter Defined as Model 2 from the Previous and Present Study along with θ Value for Comparison of Models

Model 2	Reference Study	Proposed Equation	Data Source	θ Value	
MMI-PGA	Tselentis and Danciu (2008) Worden <i>et al.</i> (2012)	MMI = 2.355 + 1.384 log PGA + 0.297 M_w - 0.832 log R	Greece	1.228	
		MMI = 0.87 + 1.55 log PGA - 0.17 M_w + 1.02 log R , log PGA \leq 1.57	California	1.268	
	Bilal and Askan (2014) This study	MMI = 2.87 + 1.47 log PGA - 0.17 M_w + 1.02 log R , log PGA > 1.57	Turkey	1.189	
		MMI = -1.692 + 0.793 log PGA + 1.653 M_w - 2.746 log R	Himalayan region	1.201	
	This study (modified) MMI-PGV (model 2) Worden <i>et al.</i> (2012)	MMI = 2.511 + 0.702 log PGA + 0.734 M_w - 1.6641 log R	Himalayan region	1.054	
		MMI = 4.68 + 1.47 log PGV - 0.18 M_w , log PGV \leq 0.53 MMI = 3.79 + 3.16 log PGV - 0.18 M_w , log PGV > 0.53	California	1.319	
	Bilal and Askan (2014) This study	MMI = 0.788 + 0.914 log PGA + 1.412 M_w - 2.904 log R	Turkey	1.164	
		MMI = 1.636 + 0.264 log PGA + 1.04 M_w - 1.821 log R	Himalayan region	1.125	
	MMI-PSA _{0.3 s}	Worden <i>et al.</i> (2012)	MMI = 0.21 + 1.69 log PSA _{0.3 s} + 0.00 M_w + 0.6 log R , log PSA _{0.3 s} \leq 2.21	California	1.305
			MMI = -5.2 + 4.14 log PSA _{0.3 s} + 0.00 M_w + 0.6 log R , log PSA _{0.3 s} > 2.21		
Bilal and Askan (2014) This study		MMI = -2.228 + 0.693 log PSA _{0.3 s} + 1.718 M_w - 2.734 log R	Turkey	1.291	
		MMI = 1.068 + 0.215 log PSA _{0.3 s} + 0.992 M_w - 1.616 log R	Himalayan region	1.258	
Atkinson and Sonley (2000) Worden <i>et al.</i> (2012)		MMI = 1.78 + 5.56 log PSA _{1.0 s} - 1.5 M_w + 1.67 log R	California	1.315	
		MMI = 4.77 + 1.51 log PSA _{1.0 s} - 0.29 M_w - 0.49 log R , log PSA _{1.0 s} \leq 1.65	California	1.257	
Bilal and Askan (2014) This study		MMI = 2.47 + 2.9 log PSA _{1.0 s} - 0.29 M_w - 0.49 log R , log PSA _{1.0 s} > 1.65	Turkey	1.201	
		MMI = -0.771 + 0.606 log PSA _{1.0 s} + 1.65 M_w - 3.131 log R	Himalayan region	1.157	
MMI-PSA _{2.0 s}		Bilal and Askan (2014) This study	MMI = 1.646 + 0.215 log PSA _{1.0 s} + 0.992 M_w - 1.7321 log R	Himalayan region	1.157
			MMI = -0.549 + 0.601 log PSA _{2.0 s} + 1.604 M_w - 3.248 log R	Turkey	1.189
MMI-PSA _{3.0 s}	Worden <i>et al.</i> (2012) This study	MMI = 0.916 + 0.257 log PSA _{2.0 s} + 0.94 M_w - 1.625 log R	Himalayan region	1.141	
		MMI = 5.72 + 1.71 log PSA _{3.0 s} - 0.21 M_w - 0.57 log R , log PSA _{3.0 s} \leq 0.99	California	1.204	
This study	This study	MMI = 3.9 + 3.01 log PSA _{3.0 s} - 0.21 M_w - 0.57 log R , log PSA _{3.0 s} > 0.99			
		MMI = 1.735 + 0.249 log PSA _{3.0 s} + 0.945 M_w - 1.648 log R	Himalayan region	1.123	

used in this study is also given in these figures for comparison. It can be seen from Figure 8a,b that the equations developed in the present study match well with Worden *et al.* (2012) and Bilal and Askan (2014), whereas the MMI versus the PGA and the MMI versus the PGV relationships developed in this study match well with the models of Faenza and Michelini (2010) and Wald *et al.* (1999), respectively. From Figure 8c, however, it is very difficult to identify quantitatively how far the present equation matches with the existing one. To compare these models quantitatively, ED has been used, as will be explained later in this section. Here, equations are developed considering MMI values up to IX, because only limited data are available for larger values. However, the derived relationships may give good predictions up to MMI X, as demonstrated in the dotted line in Figure 8.

The ED has been used in this study to compare these models statistically and quantitatively. The ED is defined as the square root of a sum of the square of the differences between N data pairs (x_i, y_i). In this study, x_i are the observed MMI values, y_i are the predicted MMI values, and ED is defined theoretically as $ED^2 = \sum_{i=1}^N (x_i - y_i)^2$. Using this

relationship, a significant trend between MMI_{obs} and MMI_{pre} can be interpreted as the biased representation of the observed data by the predicted data calculated using different empirical relationships. A new factor θ is used to measure the bias between the observed values in the region and the predicted values. The factor θ can be defined as the ratio of the original $ED_{original}$ and corrected $ED_{corrected}$ Euclidean distances. Therefore, $\theta = ED_{original}/ED_{corrected}$, in which $ED_{original}^2 = \sum_{i=1}^N (a_i - Y_i)^2$ and $ED_{corrected}^2 = \sum_{i=1}^N (a_i - Y_{ci})^2$. In these equations, a_i and Y_i are the i th observed and predicted MMI value, respectively, and N denotes the total number of observations used for the comparison. The term Y_{ci} is the corrected estimation of the i th observation after modifying Y_i as the straight line on the normal plot of the observed and predicted MMI values. Therefore, Y_{ci} is defined as $Y_{ci} = Y_i - (Y_{fit,i} - a_i)$, in which $Y_{fit,i}$ is the predicted value from the regression analysis between Y_i and a_i . The optimum value of θ would be 1, when the observed and the predicted values are close to each other. The whole procedure regarding calculation of the θ value is described in Kale and Akkar (2013).

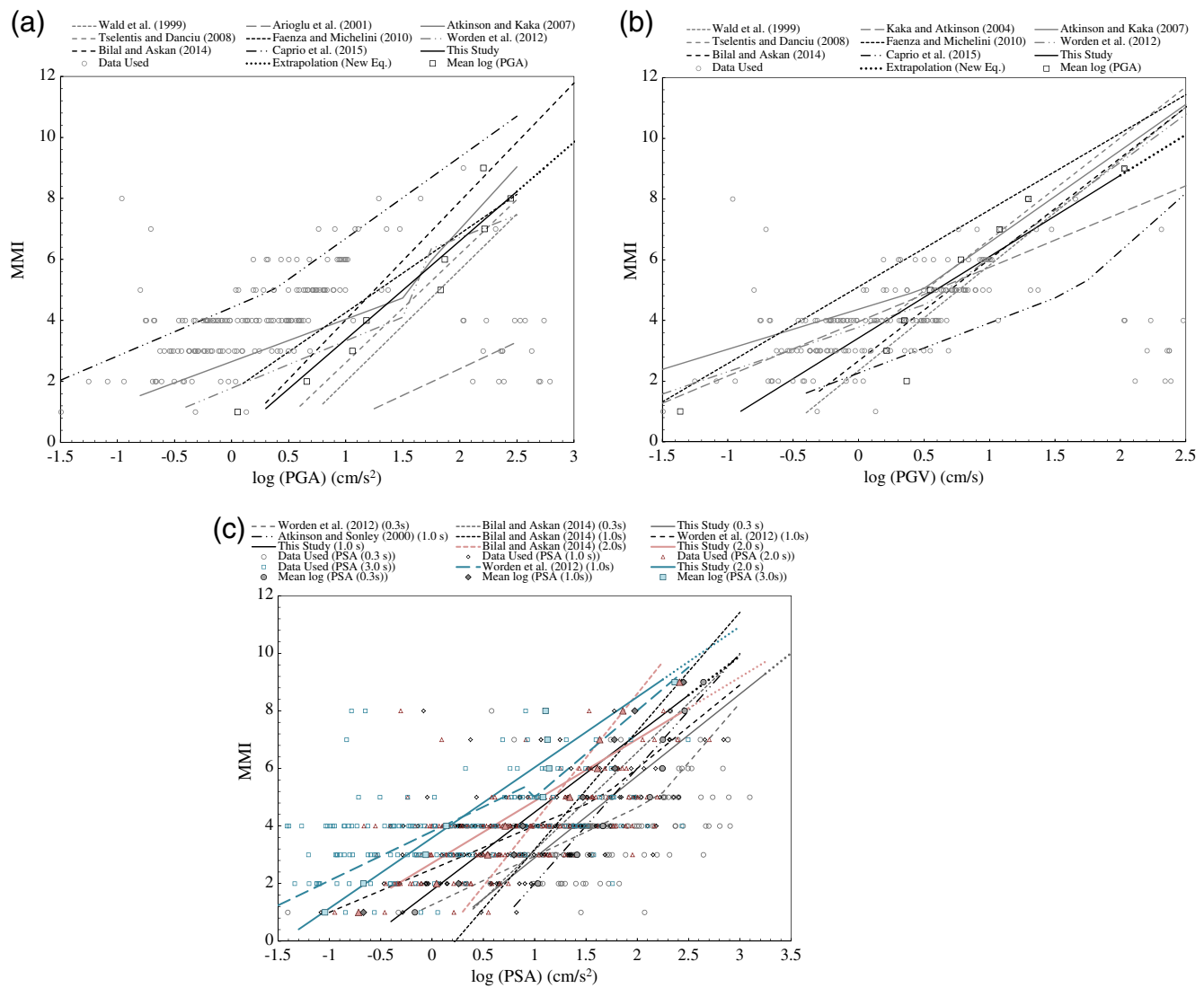


Figure 8. Comparison of (a) MMI versus PGA, (b) MMI versus PGV, and (c) MMI versus PSA at 0.3, 1.0, 2.0, and 3.0 s empirical relationships derived using model 1 in this study with other existing relationships. Thick dotted line, that is, continuation of the solid line, represents the extrapolation of the MMI values up to intensity X (MMI scale) for relationships derived in this study. The color version of this figure is available only in the electronic edition.

The MMI value was calculated based on the empirical relationship derived in the present study and given in Tables 7 and 8. Further, based on the observed MMI, the predicted or the calculated MMI was compared using EDs by calculating the θ value as explained above. It can be seen that the empirical relationship developed between the MMI and the ground-motion parameter using model 1 matches well with the empirical relationship developed by Worden *et al.* (2012) and Bilal and Askan (2014) for California and Turkey, respectively. The relationships between the MMI and the PGA and the MMI and the PGV also match well with the bilinear form of the equation developed by Faenza and Michelini (2010) considering a database of Italian earthquakes. These relationships do not match well with the relationships developed by Caprio *et al.* (2015) and Atkinson and Kaka (2007) for a worldwide database and for a central

United States and California database, respectively. The reason may be that the empirical relationship proposed by Atkinson and Kaka (2007) is derived based on simulated ground-motion parameters instead of recorded ones. The other reason may be the different style of buildings or different construction practices, as explained above. As far as the relationship between the MMI and the ground motion based on model 2 is concerned, the empirical relationship derived by Bilal and Askan (2014) matches well with the present study. Because the θ value corresponding to the MMI versus PGA relationship is less than that for the MMI versus PGV relationship, the presence of nonductile or brittle structures might be one of the reasons.

Previous studies have concluded that the MMI relates better with the PGV. Although this can be true for regions having ductile structures and longer time periods (Bilal

and Askan, 2014), in the present study area, most of the buildings are either made of rubble masonry or low-rise structures having short periods. This difference may underpin the variation in the θ value as far as the MMI versus PGV relationship is concerned. When comparing the observed MMI with the relationship developed by Worden *et al.* (2012), it can be seen that it matches well at an MMI value of 5, but for higher observed MMI values the difference is considerable. Because these relationships were developed for the California region in which most of the structures are earthquake resistant, a lower MMI value will be observed for the same ground shaking in the study area. This might be one of the reasons for the large difference in the θ value compared to the present study. The difference in the MMI value calculated from various studies may also be due to different building and damage styles and the variability in ground-motion characteristics, that is, the frequency content and duration in different regions. Based on this analysis, it can be seen that large variations in the PGV values correspond to similar MMI values. It can be concluded that the MMI versus PGV relationship is region specific, because it depends upon various regional characteristics and also the type and dimension of a structure, and because the energy dissipated by the structural component is a function of velocity as explained earlier. It can be also noted here that the equations derived in this study for the Himalayan region are valid up to an MMI of IX, because for the MMI values of more than IX, a strong ground motion database is not available. Extrapolation of the proposed equation predicts up to an intensity of X in the MMI scale (Fig. 8).

These relationships can be used for other regions following proper quantitative assessment of their suitability. Additionally, it can be stated that regionally specific empirical relationships between the MMI and the ground-motion parameters need to be used to determine the ShakeMap or the estimation of loss. The empirical relationships derived based on model 3 are recommended for future study, because the regional dependency has been removed in this model by including the moment magnitude, the distance, and the site condition.

Conclusion

In this study, an empirical relationship between the MMI and the ground-motion parameters has been derived for the Himalayan region using three models. First, the MMI is related only to the ground-motion parameters such as the PGA and the PSA at 0.3, 1.0, 2.0, and 3.0 s; second, hypocentral distance and magnitude were included as independent variables; and third, the site effect based on shear-wave velocity at 30 m depth V_{S30} was used as a potential independent parameter. An extensive ground-motion database from 21 earthquakes was used with corresponding uniform macroseismic intensity in the MMI scale. The residual difference is greater when calculating the MMI as dependent on the PGA using model 2 compared to using model 3. This may

be due to the site effect and the type of structures. Therefore, it can be concluded that the MMI can be determined using the ground-motion parameters along with V_{S30} to account for the site effect. It was further found that incorporating the site-specific shear-wave velocity assists in accounting for the site and the building effects in predicting the MMI considering the PGA, although this information is not available for many of the sites. To counterbalance the site effect for the sites where V_{S30} is not easily available, the relationship between observed and predicted MMI was calculated with or without V_{S30} as a potential independent variable. However, most of the data used in this study are for site classes B, C, and D. Furthermore, the empirical correlations were derived for an intensity of IX (MMI scale), although they predict acceptable results up to a macroseismic intensity of X (MMI scale). Additionally, the concept of ED is used to compare the existing MMI and the ground-motion relationships with the empirical relationship developed in this study. It was seen that the θ value varies more in the case of the PGV and the PSA (different time periods) compared to the PGA, considering the existing and presently derived empirical relationships. It was, therefore, concluded that the PGA is a good indicator for deriving the MMI value in the Himalayan region, but that one should use site-specific MMI versus PGV and MMI versus PSA relationships to predict reliable parameters.

Data and Resources

The processed ground-motion parameters for earthquakes before 2005 are obtained from the Strong-Motion Virtual Data Center (VDC), which was developed by the University of California Santa Barbara and incorporated as a part of the Center for Engineering Strong Motion Data at <http://strongmotioncenter.org/vdc> (last accessed August 2015). From the 192 ground-motion recordings, 124 are collected from the strong-motion instrumentation network of Indian Institute of Technology, Roorkee (IITR), that covers the Indian Himalayan range from Jammu and Kashmir to Meghalaya. These data are freely available and downloaded from the website <http://www.pesmos.in> (last accessed August 2015). The majority of the isoseismal maps used in this study are taken from a book, "Microearthquake Seismology and Seismotectonics of South Asia," written by J. R. Kayal in 2008. These maps are scanned and then digitized to get the intensity data for most of the earthquakes occurring in the Himalayan region. The "Did You Feel It?" (DYFI) data used in this study are freely available to download from the archive at <http://earthquake.usgs.gov/dyfi/> (last accessed August 2015). Building damage reports from the Garhwal earthquake (1991) and the Chamoli earthquake (1999) have been used to understand the construction practices and damage to structures due to these earthquakes. These reports are available online at http://www.nicee.org/eqe-iitk/uploads/EQR_Uttarkashi.pdf (last accessed August 2015) and http://www.nicee.org/eqe-iitk/uploads/EQR_Chamoli.pdf (last accessed August 2015), respectively, for the Garhwal and the Chamoli earthquakes.

Acknowledgments

The authors would like to thank the anonymous reviewers for their valuable comments in improving the article. The first author thanks the Science and Engineering Research Board (SERB), Department of Science and Technology (DST), India, for funding the project titled, "Measurement of Shear Wave Velocity at Deep Soil Sites and Site Response Studies," Ref: SERB/F/162/2015-2016. The authors extend their sincere appreciation to the Deanship of Scientific Research at the King Saud University for funding this Prolific Research Group (PRG-1436-06).

References

- Akansel, V., G. Ameri, A. Askan, A. Caner, B. Erdil, O. Kale, and D. Okuyucu (2013). The 23 October 2011 M_w 7.0 Van (Eastern Turkey) earthquake: Interpretations of recorded strong ground motions and post-earthquake conditions of nearby structures, *Earthq. Spectra* **30**, no. 2, 657–682, doi: [10.1193/012912EQS020M](https://doi.org/10.1193/012912EQS020M).
- Arioglu, E., B. Arioglu, and C. Girgin (2001). Assessment of the eastern Marmara earthquake in terms of acceleration values, *Beton Prefabrikasyon* **57**, 5–15.
- Atkinson, G. M., and S. I. Kaka (2007). Relationships between felt intensity and instrumental ground motion in the central United States and California, *Bull. Seismol. Soc. Am.* **97**, no. 2, 497–510.
- Atkinson, G. M., and E. Sonley (2000). Empirical relationships between modified Mercalli intensity and response spectra, *Bull. Seismol. Soc. Am.* **90**, 537–544.
- Atkinson, G. M., and D. J. Wald (2007). "Did You Feel It?" intensity data: A surprisingly good measure of earthquake ground motion, *Seismol. Res. Lett.* **78**, 362–368.
- Bilal, M., and A. Askan (2014). Relationship between felt intensity and recorded ground-motion parameters for Turkey, *Bull. Seismol. Soc. Am.* **104**, 484–496.
- Bilham, R. (2015). Raising Kathmandu, *Nat. Geosci.* **8**, 582–584.
- Bilham, R., and V. K. Gaur (2000). The geodetic contribution to Indian seismotectonics, *Curr. Sci.* **79**, no. 9, 1259–1269.
- Bilham, R., F. Blume, R. Bendick, and V. K. Gaur (1998). The geodetic constraints on the translation and deformation of India: Implications for future great Himalayan earthquakes, *Curr. Sci.* **74**, 213–229.
- Boatwright, J., K. Thywissen, and L. C. Seekins (2001). Correlation of ground motion and intensity for the 17 January 1994 Northridge, California, earthquake, *Bull. Seismol. Soc. Am.* **91**, 739–752.
- Breusch, T. S., and A. R. Pagan (1979). A simple test for heteroscedasticity and random coefficient variation, *Econometrica* **47**, 1287–1294.
- Caprio, M., B. Tarigan, B. C. Worden, S. Wiemer, and D. J. Wald (2015). Ground motion to intensity conversion equations (GMICES): A global relationship and evaluation of regional dependency, *Bull. Seismol. Soc. Am.* **105**, 1476–1490.
- de Groen, P. P. N. (1996). An introduction to total least squares, *Nieuw Arch. Wisk.* **14**, no. 2, 237–254.
- Deming, W. E. (1943). *Statistical Adjustment of Data*, Wiley, New York, New York.
- Durbin, J., and G. S. Watson (1950). Testing for serial correlation in least squares regression I, *Biometrika* **37**, 409–428.
- Earle, P. S., D. J. Wald, K. S. Jaiswal, T. I. Allen, K. D. Marano, A. J. Hotovec, M. G. Hearne, and J. M. Fee (2009). Prompt assessment of global earthquakes for response (PAGER): A system for rapidly determining the impact of global earthquakes worldwide, *U.S. Geol. Surv. Open-File Rept. 2009-1131*, 15 pp.
- Faenza, L., and A. Michelini (2010). Regression analysis of MCS intensity and ground motion parameters in Italy and its application in Shake-Map, *Geophys. J. Int.* **180**, 1138–1152.
- Gansser, A. (1964). *Geology of the Himalayas*, Interscience, New York, New York, 289 pp.
- Ghofrani, H., and G. M. Atkinson (2014). Site condition evaluation using horizontal-to-vertical response spectral ratios of earthquakes in the

A. Panjamani, K. Bajaj, S. S. R. Moustafa, and N. S. N. Al-Arifi

- NGA-West 2 and Japanese databases, *Soil Dynam. Earthq. Eng.* **67**, 30–43.
- Gutenberg, B., and C. F. Richter (1956). Earthquake magnitude, intensity, energy, and acceleration, *Bull. Seismol. Soc. Am.* **46**, no. 2, 105–145.
- Hershberger, J. (1956). A comparison of earthquake accelerations with intensity ratings, *Bull. Seismol. Soc. Am.* **46**, no. 4, 317–320.
- Jain, S. K., C. V. R. Murty, J. N. Arlekar, C. P. Rajendran, K. Rajendran, and R. Sinha (1999). Chamoli (Himalaya, India) earthquake of 29 March 1999, *EERI Special Earthquake Rept.*, EERI Newsletter, Vol. **33**, no. 7, Oakland, California.
- Jain, S. K., R. P. Singh, V. K. Gupta, and A. Nagar (1992). Garhwal earthquake of Oct. 1991, *EERI Special Earthquake Rept.*, EERI Newsletter, Vol. **26**, no. 2, Oakland, California.
- Kaka, S. I., and G. M. Atkinson (2004). Relationships between instrumental ground-motion parameters and modified Mercalli intensity in eastern North America, *Bull. Seismol. Soc. Am.* **94**, no. 5, 1728–1736.
- Kale, O., and S. Akkar (2013). A New procedure for selecting and ranking ground-motion prediction equation (GMPEs): The Euclidean distance-based ranking (EDR) method, *Bull. Seismol. Soc. Am.* **103**, no. 2A, 1069–1084.
- Kamer, Y., E. Abdulhamitbilal, M. B. Demircioglu, M. Erdik, U. Hancilar, K. Sesetyan, C. Yenidogan, and A. C. Zulfikar (2009). *Earthquake Loss Estimation Routine ELER v.1.0 User Manual*, Bogazici University, Department of Earthquake Engineering, Istanbul, Turkey.
- Kayal, J. R. (2008). *Microearthquake Seismology and Seismotectonics of South Asia*, Springer, New Delhi, India.
- Khattri, K. N. (1999). An evaluation of earthquake hazard and risk in northern India, *Himalayan Geol.* **20**, 1–46.
- Kumar, A., H. Mittal, R. Sachdeva, and A. Kumar (2012). Indian strong motion instrumentation network, *Seismol. Res. Lett.* **83**, 59–66.
- Mahajan, A. K., and N. S. Virdi (2001). Macroseismic field generated by 29 March, 1999 Chamoli earthquake and its seismotectonics, *J. Asian Earth Sci.* **19**, 507–516.
- Markovsky, I., and S. Van Huffel (2007). Overview of total least-squares methods, *Signal Process.* **87**, 2283–2302.
- McCann, M. W., F. Sauter, and H. C. Shah (1980). A technical note on PGA-intensity relations with applications to damage estimation, *Bull. Seismol. Soc. Am.* **70**, no. 2, 631–637.
- Molnar, P., and W. P. Chen (1982). Seismicity and mountain building, in *Mountain Building Processes*, K. Hsu (Editor), Academic Press, New York, New York, 41–57.
- Murphy, J. R., and L. J. O'Brien (1977). The correlation of peak ground acceleration amplitude with seismic intensity and other physical parameters, *Bull. Seismol. Soc. Am.* **67**, 877–915.
- Musson, R. M. W., G. Grünthal, and M. Stucchi (2010). The comparison of macroseismic intensity scales, *J. Seismol.* **14**, 413–428.
- Nath, S. K., and K. K. S. Thingbaijam (2011). Peak ground motion predictions in India: An appraisal for rock sites, *J. Seismol.* **15**, 295–315.
- Parameswaran, R. M., T. Natarajan, K. Rajendran, C. P. Rajendran, R. Mallick, M. Wood, and H. C. Lekhak (2015). Seismotectonics of the April–May 2015 Nepal earthquakes: An assessment based on the aftershock patterns, surface effects and deformational characteristics, *J. Asian Earth Sci.* **111**, 161–174.
- Prasad, J. S. R., Y. Singh, A. M. Kaynia, and C. Lindholm (2009). Socio-economic clustering in seismic risk assessment of urban housing stock, *Earthq. Spectra* **25**, 619–641.
- Rajendran, C. P., B. John, and K. Rajendran (2015). Medieval pulse of great earthquakes in the central Himalayan: Viewing past activities on the frontal thrust, *J. Geophys. Res. Solid Earth* **120**, 1623–1641.
- Reiter, L. (1990). *Earthquake Hazard Analysis*, Columbia University Press, New York, New York, 254 pp.
- Seeber, L., and J. G. Armbruster (1981). Great detachment earthquakes along the Himalayan arc and long-term forecasting, in *Earthquake Prediction: An International Review*, M. Ewing (Editor), Series 4, American Geophysical Union, Washington, D.C., 259–277.
- Shah, H., R. Boyle, and W. Dong (1991). Geographic information systems and artificial intelligence: An application for seismic zonation, *Proc. of*

- the Fourth International Conf. on Seismic Zonation, Vol. I, Stanford, California, 25–29 August 1991, 487–517.
- Singh, S. K., W. K. Mohanty, B. K. Bansal, and G. S. Roonwal (2002). Ground motion in Delhi from future large/great earthquakes in the central seismic gap of the Himalayan arc, *Bull. Seismol. Soc. Am.* **92**, 555–569.
- Spence, R., A. Coburn, and A. Pomonis (1992). Correlation of ground motion with building damage: The definition of a new damage-based seismic intensity scale, *Proc. of the Tenth World Conf. on Earthquake Engineering*, Vol. 1, Madrid, Spain, 551–556.
- Trendafiloski, G., M. Wyss, and P. Rosset (2011). Loss estimation module in the second generation software QLARM, *Proc. of the Second International Workshop on Disaster Casualties June 2009*, Cambridge, United Kingdom.
- Tselentis, G., and L. Danciu (2008). Empirical relationships between modified Mercalli intensity and engineering ground-motion parameters in Greece, *Bull. Seismol. Soc. Am.* **98**, no. 4, 1863–1875.
- Wald, D. J., V. Quitoriano, T. H. Heaton, and H. Kanamori (1999). Relationships between peak ground acceleration, peak ground velocity and modified Mercalli intensity in California, *Earthq. Spectra* **15**, 557–564.
- Wald, D. J., V. Quitoriano, C. B. Worden, M. Hopper, and J. W. Dewey (2011). USGS “Did You Feel It?” internet-based macroseismic intensity maps, *Ann. Geophys.* **54**, no. 6, 688–709.
- Worden, C. B., M. C. Gerstenberger, D. A. Rhoades, and D. J. Wald (2012). Probabilistic relationships between ground-motion parameters and modified Mercalli intensity in California, *Bull. Seismol. Soc. Am.* **102**, no. 1, 204–221.

Department of Civil Engineering
Indian Institute of Science
Bangalore 560012, India
anbu@civil.iisc.ernet.in
16ketan1990@gmail.com
(A.P., K.B.)

Geology and Geophysics Department
Faculty of Science, King Saud University
Riyadh 11451, Saudi Arabia
smoustafa@ksu.edu.sa
nalarifi@ksu.edu.sa
(S.S.R.M., N.S.N.A.-A.)

Manuscript received 27 November 2015;
Published Online 21 July 2016